

Measurement of the virtual-photon asymmetry A_2 and the spin-structure function g_2 of the proton

The HERMES Collaboration

A. Airapetian^{12,15}, N. Akopov²⁶, Z. Akopov⁵, E.C. Aschenauer^{6,a}, W. Augustyniak²⁵, R. Avakian²⁶, A. Avetissian²⁶, E. Avetisyan⁵, S. Belostotski¹⁸, N. Bianchi¹⁰, H.P. Blok^{17,24}, A. Borissov⁵, J. Bowles¹³, V. Bryzgalov¹⁹, J. Burns¹³, M. Capiluppi⁹, G.P. Capitani¹⁰, E. Cisbani²¹, G. Ciullo⁹, M. Contalbrigo⁹, P.F. Dalpiaz⁹, W. Deconinck⁵, R. De Leo², L. De Nardo^{11,5}, E. De Sanctis¹⁰, M. Diefenthaler^{14,8}, P. Di Nezza¹⁰, M. Düren¹², M. Ehrenfried¹², G. Elbakian²⁶, F. Ellinghaus⁴, A. Fantoni¹⁰, L. Felawka²², S. Frullani²¹, D. Gabbert⁶, G. Gapienko¹⁹, V. Gapienko¹⁹, F. Garibaldi²¹, G. Gavrilo^{5,18,22}, V. Gharibyan²⁶, F. Giordano^{5,9}, S. Gliske¹⁵, M. Golembiovskaya⁶, C. Hadjidakis¹⁰, M. Hartig⁵, D. Hasch¹⁰, A. Hillenbrand⁶, M. Hoek¹³, Y. Holler⁵, I. Hristova⁶, Y. Imazu²³, A. Ivanilov¹⁹, H.E. Jackson¹, H.S. Jo¹¹, S. Joosten¹⁴, R. Kaiser^{13,b}, G. Karyan²⁶, T. Keri^{13,12}, E. Kinney⁴, A. Kisselev¹⁸, V. Korotkov¹⁹, V. Kozlov¹⁶, P. Kravchenko^{8,18}, V.G. Krivokhijine⁷, L. Lagamba², L. Lapikás¹⁷, I. Lehmann¹³, P. Lenisa⁹, A. López Ruiz¹¹, W. Lorenzon¹⁵, B.-Q. Ma³, D. Mahon¹³, N.C.R. Makins¹⁴, S.I. Manaenkov¹⁸, L. Manfré²¹, Y. Mao³, B. Marianski²⁵, A. Martinez de la Ossa^{5,4}, H. Marukyan²⁶, C.A. Miller²², Y. Miyachi^{23,c}, A. Movsisyan²⁶, V. Muccifora¹⁰, M. Murray¹³, A. Mussgiller^{5,8}, E. Nappi², Y. Naryshkin¹⁸, A. Nass⁸, M. Negodaev⁶, W.-D. Nowak⁶, L.L. Pappalardo⁹, R. Perez-Benito¹², A. Petrosyan²⁶, P.E. Reimer¹, A.R. Reolon¹⁰, C. Riedl⁶, K. Rith⁸, G. Rosner¹³, A. Rostomyan⁵, J. Rubin^{1,14}, D. Ryckbosch¹¹, Y. Salomatin¹⁹, F. Sanftl^{23,20}, A. Schäfer²⁰, G. Schnell^{6,11,d}, K.P. Schuler⁵, B. Seitz¹³, T.-A. Shibata²³, V. Shutov⁷, M. Stancari⁹, M. Statera⁹, E. Steffens⁸, J.J.M. Steijger¹⁷, J. Stewart⁶, F. Stinzing⁸, S. Taroian²⁶, A. Terkulov¹⁶, R. Truty¹⁴, A. Trzcinski²⁵, M. Tytgat¹¹, A. Vandenbroucke¹¹, Y. Van Haarlem¹¹, C. Van Hulse¹¹, D. Veretennikov¹⁸, V. Vikhrov¹⁸, I. Vilardi², S. Wang³, S. Yaschenko^{6,8}, Z. Ye⁵, S. Yen²², V. Zagrebelnyy^{5,12}, D. Zeiler⁸, B. Zihlmann⁵, P. Zupranski²⁵

¹Physics Division, Argonne National Laboratory, Argonne, Illinois 60439-4843, USA

²Istituto Nazionale di Fisica Nucleare, Sezione di Bari, 70124 Bari, Italy

³School of Physics, Peking University, Beijing 100871, China

⁴Nuclear Physics Laboratory, University of Colorado, Boulder, Colorado 80309-0390, USA

⁵DESY, 22603 Hamburg, Germany

⁶DESY, 15738 Zeuthen, Germany

⁷Joint Institute for Nuclear Research, 141980 Dubna, Russia

⁸Physikalisches Institut, Universität Erlangen-Nürnberg, 91058 Erlangen, Germany

⁹Istituto Nazionale di Fisica Nucleare, Sezione di Ferrara and Dipartimento di Fisica, Università di Ferrara, 44100 Ferrara, Italy

¹⁰Istituto Nazionale di Fisica Nucleare, Laboratori Nazionali di Frascati, 00044 Frascati, Italy

¹¹Department of Physics and Astronomy, Ghent University, 9000 Gent, Belgium

¹²Physikalisches Institut, Universität Gießen, 35392 Gießen, Germany

¹³SUPA, School of Physics and Astronomy, University of Glasgow, Glasgow G12 8QQ, United Kingdom

¹⁴Department of Physics, University of Illinois, Urbana, Illinois 61801-3080, USA

¹⁵Randall Laboratory of Physics, University of Michigan, Ann Arbor, Michigan 48109-1040, USA

¹⁶Lebedev Physical Institute, 117924 Moscow, Russia

¹⁷National Institute for Subatomic Physics (Nikhef), 1009 DB Amsterdam, The Netherlands

^a Now at: Brookhaven National Laboratory, Upton, New York 11772-5000, USA

^b Present address: International Atomic Energy Agency, A-1400 Vienna, Austria

^c Now at: Department of Physics, Yamagata University, Yamagata 990-8560, Japan

^d Now at: Department of Theoretical Physics, University of the Basque Country UPV/EHU, 48080 Bilbao, Spain and IKERBASQUE, Basque Foundation for Science, 48011 Bilbao, Spain

¹⁸Petersburg Nuclear Physics Institute, Gatchina, 188300 Leningrad Region, Russia

¹⁹Institute for High Energy Physics, Protvino, 142281 Moscow Region, Russia

²⁰Institut für Theoretische Physik, Universität Regensburg, 93040 Regensburg, Germany

²¹Istituto Nazionale di Fisica Nucleare, Sezione di Roma, Gruppo Collegato Sanità and Istituto Superiore di Sanità, 00161 Roma, Italy

²²TRIUMF, Vancouver, British Columbia V6T 2A3, Canada

²³Department of Physics, Tokyo Institute of Technology, Tokyo 152, Japan

²⁴Department of Physics and Astronomy, VU University, 1081 HV Amsterdam, The Netherlands

²⁵National Centre for Nuclear Research, 00-689 Warsaw, Poland

²⁶Yerevan Physics Institute, 375036 Yerevan, Armenia

Received: March 30, 2018/ Revised version:

Abstract. A measurement of the virtual-photon asymmetry $A_2(x, Q^2)$ and of the spin-structure function $g_2(x, Q^2)$ of the proton are presented for the kinematic range $0.004 < x < 0.9$ and $0.18 \text{ GeV}^2 < Q^2 < 20 \text{ GeV}^2$. The data were collected by the HERMES experiment at the HERA storage ring at DESY while studying inclusive deep-inelastic scattering of 27.6 GeV longitudinally polarized leptons off a transversely polarized hydrogen gas target. The results are consistent with previous experimental data from CERN and SLAC. For the x -range covered, the measured integral of $g_2(x)$ converges to the null result of the Burkhardt–Cottingham sum rule. The x^2 moment of the twist-3 contribution to $g_2(x)$ is found to be compatible with zero.

The description of inclusive deep-inelastic scattering of longitudinally polarized charged leptons off polarized nucleons requires two nucleon spin-structure functions, $g_1(x, Q^2)$ and $g_2(x, Q^2)$, in addition to the well-known structure functions $F_1(x, Q^2)$ and $F_2(x, Q^2)$ [1]. Here, $-Q^2$ is the squared four-momentum of the exchanged virtual photon with laboratory energy ν , $x = Q^2/(2M\nu)$ is the Bjorken scaling variable, and M is the nucleon mass. In the quark-parton model (QPM), the spin structure function $g_1(x, Q^2)$ can be interpreted as a charge-weighted sum of the quark helicity distributions $\Delta q(x, Q^2)$ describing a longitudinally polarized nucleon,

$$g_1(x, Q^2) = \frac{1}{2} \sum_q e_q^2 \Delta q(x, Q^2). \quad (1)$$

The spin structure function $g_2(x, Q^2)$ does not have such a probabilistic interpretation in the QPM. Its properties can be interpreted in the framework of the operator product expansion (OPE) analysis [2, 3, 4], which shows that $g_2(x, Q^2)$ is related to the matrix elements of both twist-2 and twist-3 operators. Neglecting quark mass effects, $g_2(x, Q^2)$ can be written as a sum of two terms

$$g_2(x, Q^2) = g_2^{\text{WW}}(x, Q^2) + \bar{g}_2(x, Q^2). \quad (2)$$

Here, $g_2^{\text{WW}}(x, Q^2)$ is the twist-2 part derived by Wandzura and Wilczek [5]

$$g_2^{\text{WW}}(x, Q^2) = -g_1(x, Q^2) + \int_x^1 g_1(y, Q^2) \frac{dy}{y}. \quad (3)$$

The second term in Eq. (2), $\bar{g}_2(x, Q^2)$, is the twist-3 part of $g_2(x, Q^2)$. It arises from quark-gluon correlations in the nucleon and is the most interesting part of the function. The x^2 moment of $\bar{g}_2(x, Q^2)$,

$$d_2(Q^2) = 3 \int_0^1 x^2 \bar{g}_2(x, Q^2) dx, \quad (4)$$

can be calculated on the lattice (see, *e.g.*, [6, 7], where d_2 is defined with an additional factor of two with respect to (4)). The moment d_2 has also been linked to the transverse force acting on the quark that absorbed the virtual photon in a transversely polarized nucleon, and thus to the Sivers effect [8, 9, 10].

The Burkhardt–Cottingham sum rule [11] for g_2 at large Q^2 ,

$$\int_0^1 g_2(x, Q^2) dx = 0, \quad (5)$$

does not follow from the OPE. Its validity relies on an assumed Regge behaviour of g_2 at low x . In the absence of higher twist contributions to the function g_2 , *i.e.*, $\bar{g}_2(x) \equiv 0$, the sum rule would automatically be fulfilled. Hence a violation of the sum rule would indicate the presence of higher-twist contributions.

The spin structure functions $g_1(x, Q^2)$ and $g_2(x, Q^2)$ can be related to the virtual photon-absorption asymmetries $A_1(x, Q^2)$ and $A_2(x, Q^2)$ [1]

$$A_1 = \frac{\sigma_{1/2}^{\mathcal{T}} - \sigma_{3/2}^{\mathcal{T}}}{\sigma_{1/2}^{\mathcal{T}} + \sigma_{3/2}^{\mathcal{T}}} = \frac{g_1 - \gamma^2 g_2}{F_1}, \quad (6)$$

$$A_2 = \frac{2\sigma^{\mathcal{LT}}}{\sigma_{1/2}^{\mathcal{T}} + \sigma_{3/2}^{\mathcal{T}}} = \gamma \frac{g_1 + g_2}{F_1}. \quad (7)$$

Here, $\sigma_{1/2}^{\mathcal{T}}$ and $\sigma_{3/2}^{\mathcal{T}}$ are the transverse virtual-photon absorption cross sections for total photon plus nucleon angular momentum projection on the photon direction of 1/2 and 3/2, respectively. The cross-section $\sigma^{\mathcal{LT}}$ arises from the interference between the transverse and longitudinal photon-nucleon amplitudes, with $\gamma = 2Mx/\sqrt{Q^2}$. All of the σ 's are differential cross sections depending on x and Q^2 , but this dependence was omitted for brevity.

The measurement of the structure function g_2 requires a longitudinally polarized beam and a transversely po-

larized target. In this case, the inclusive differential cross section can be represented as a sum of two terms, the polarization-averaged part, σ_{UU} , and the polarization-related part, σ_{LT} . Here, the subscript UU indicates that both the beam and the target are unpolarized, while the subscript LT indicates a longitudinally polarized beam and a transversely polarized target. The polarization-related part of the cross section at Born level, *i.e.*, in the one-photon approximation, is given by [3]

$$\frac{d^3\sigma_{LT}}{dx dy d\phi} = -h_l \cos\phi \frac{4\alpha^2}{Q^2} \gamma \sqrt{1-y-\frac{\gamma^2 y^2}{4}} \times \left(\frac{y}{2} g_1(x, Q^2) + g_2(x, Q^2) \right). \quad (8)$$

Here, $h_l = +1$ (-1) for a lepton beam with positive (negative) helicity, α is the fine-structure constant, and $y = \nu/E$, where E is the incident lepton energy. The angle ϕ is the azimuthal angle about the beam direction between the lepton scattering plane and the ‘‘upwards’’ target spin direction. The polarization-related cross section σ_{LT} is significantly smaller than the polarization-averaged part σ_{UU} and therefore its measurement requires high statistical precision. Up to now, the function g_2 and the asymmetry A_2 have been extracted [12, 13, 14] to less accuracy than g_1 and A_1 .

A measurement of the inclusive cross sections (8) at angles ϕ and $\phi + \pi$ allows one to construct the asymmetry A_{LT} ,

$$A_{LT}(x, Q^2, \phi) = h_l \frac{\sigma(x, Q^2, \phi) - \sigma(x, Q^2, \phi + \pi)}{\sigma(x, Q^2, \phi) + \sigma(x, Q^2, \phi + \pi)} = h_l \frac{\sigma_{LT}(x, Q^2, \phi)}{\sigma_{UU}(x, Q^2, \phi)} = -A_T(x, Q^2) \cos\phi, \quad (9)$$

which defines the asymmetry amplitude $A_T(x, Q^2)$. This amplitude contains all information on the function g_2 and the asymmetry A_2 . Their extraction requires the knowledge of $\sigma_{UU}(x, Q^2)$, which can be expressed by the structure functions $F_{1,2}(x, Q^2)$ or, equivalently, parameterizations of the function $F_2(x, Q^2)$ and the ratio of longitudinal to transverse virtual-photon absorption cross sections $R = R(x, Q^2)$. The extraction of the structure function $g_2(x, Q^2)$ from the asymmetry amplitude A_T is analogous to the extraction of $g_1(x, Q^2)$ from the longitudinal asymmetry as described in [15]. The function g_2 can be extracted from the measured asymmetry amplitude A_T and parameterizations of previous measurements of σ_{UU} and g_1 , using (8) and (9). Also F_1 can be computed from parameterizations of F_2 and R . This leads with (7) to the following relations

$$g_2 = \frac{F_1}{\gamma(1+\gamma\xi)} \left(\frac{A_T}{d} - (\gamma - \xi) \frac{g_1}{F_1} \right), \quad (10)$$

$$A_2 = \frac{1}{1+\gamma\xi} \left(\frac{A_T}{d} + \xi(1+\gamma^2) \frac{g_1}{F_1} \right), \quad (11)$$

with

$$d = \frac{\sqrt{1-y-\gamma^2 y^2/4}}{(1-y/2)} D, \quad (12)$$

$$\xi = \frac{\gamma(1-y/2)}{(1+\gamma^2 y/2)}, \quad (13)$$

$$D = \frac{y(2-y)(1+\gamma^2 y/2)}{y^2(1+\gamma^2) + 2(1-y-\gamma^2 y^2/4)(1+R)}. \quad (14)$$

However, it is not obvious from these relations that the extraction of g_2 is independent of correlated variations in values of F_1 , F_2 and R that conserve the directly measured values of σ_{UU} .

This paper reports a new measurement of the function g_2 and the asymmetry A_2 . The data were collected during the years 2003 – 2005 with the HERMES spectrometer [16] using a longitudinally polarized positron or electron beam of energy 27.6 GeV scattered off a transversely polarized target [17] of pure hydrogen gas internal to the HERA lepton storage ring at DESY. The usage of a pure target avoids the complications of nuclear corrections present in previous measurements. The open-ended target cell was fed by an atomic-beam source [18] based on Stern–Gerlach separation combined with radio-frequency transitions between hydrogen hyperfine states. The nuclear polarization of the atoms was flipped at 1–3 minute time intervals, while both the polarization magnitude and the atomic fraction inside the target cell were continuously measured [19]. The average magnitude of the proton polarization was 0.78 ± 0.04 . The lepton beam (positrons during 2003 – 2004 and electrons in 2005) was self-polarized in the transverse direction due to the asymmetry in the emission of synchrotron radiation [20] in the arcs of the HERA storage ring. Longitudinal orientation of the beam polarization was obtained by using a pair of spin rotators [21] located before and after the interaction region of the HERMES spectrometer. The sign of the beam polarization was reversed every few months. The beam polarization was measured by two independent HERA polarimeters [22, 23, 24]. The average magnitude of the beam polarization was found to be 0.34 ± 0.01 . The scattered leptons were detected by the HERMES spectrometer within an angular acceptance of ± 170 mrad horizontally and $\pm(40 - 140)$ mrad vertically. The leptons were identified using the information from an electromagnetic calorimeter, a transition-radiation detector, a preshower scintillating counter and a dual-radiator ring-imaging Čerenkov detector. The identification efficiency for leptons with momentum larger than 2.5 GeV exceeds 98%, while the hadron contamination in the lepton sample is found to be less than 1%. The luminosity monitor [25] measured e^+e^- (e^-e^-) pairs from Bhabha (Møller) scattering of beam positrons (electrons) off the target gas electrons, and $\gamma\gamma$ pairs from e^+e^- annihilation in two NaBi(WO₄)₂ electromagnetic calorimeters, which were mounted symmetrically on either side of the beam line. Tracking corrections were applied for the deflections of the scattered particles caused by the vertical 0.3 T target

holding field, with little effect on the extracted asymmetries.

Most of the details of the analysis follow the inclusive analysis described in [15]. The kinematic constraints imposed on the events were: $0.18 \text{ GeV}^2 < Q^2 < 20 \text{ GeV}^2$, invariant mass of the virtual photon–nucleon system $W > 1.8 \text{ GeV}$, $0.004 < x < 0.9$, and $0.10 < y < 0.91$. After applying data quality criteria, 10.2×10^6 events were available for the asymmetry analysis. The kinematic region covered by the experiment in (x, Q^2) -space was divided into nine bins in x . Each of the seven x -bins in the region $x > 0.023$ was subdivided into three logarithmically equidistant bins in Q^2 . The range in ϕ -space (2π) was divided into 10 bins. Two of the ϕ -bins cover the shielding steel-plate region of the spectrometer and thus cannot be used for the analysis. The data were corrected for the e^+e^- charge-symmetric background [15], which amounted in total to about 1.8% of the events, reaching the largest contribution of about 14% at small values of x .

The measurement of the asymmetry $A_{LT}(x, Q^2, \phi)$ given by (9) can be performed by either reversing the transverse target polarization and comparing the number of events in the same part of the detector, or by comparing the number of events in the upper and lower part of the detector for the same upward or downward target polarization direction. The first method provides a better cancellation of acceptance effects and was chosen to obtain the asymmetry

$$A_{LT}(x, Q^2, \phi, h_l) = h_l \frac{N^{h_l \uparrow}(x, Q^2, \phi) \mathcal{L}^{h_l \downarrow} - N^{h_l \downarrow}(x, Q^2, \phi) \mathcal{L}^{h_l \uparrow}}{N^{h_l \uparrow}(x, Q^2, \phi) \mathcal{L}_p^{h_l \downarrow} + N^{h_l \downarrow}(x, Q^2, \phi) \mathcal{L}_p^{h_l \uparrow}}. \quad (15)$$

Here, $N^{h_l \uparrow(\downarrow)}$ is the number of scattered leptons in one bin of the 3-dimensional space (x, Q^2, ϕ) for the case of the incident lepton with helicity h_l when the direction of the proton spin points up (down). $\mathcal{L}^{h_l \uparrow(\downarrow)}$ and $\mathcal{L}_p^{h_l \uparrow(\downarrow)}$ are the corresponding integrated luminosities and the integrated luminosities weighted with the absolute value of the beam and target polarization product, respectively

$$\mathcal{L}^{h_l \uparrow(\downarrow)} = \int dt L^{h_l \uparrow(\downarrow)}(t) \tau(t), \quad (16)$$

$$\mathcal{L}_p^{h_l \uparrow(\downarrow)} = \int dt L^{h_l \uparrow(\downarrow)}(t) |P_B(t) P_T(t)| \tau(t). \quad (17)$$

Here, $L(t)$ is the luminosity, $\tau(t)$ is the trigger live-time factor, and P_B and P_T are the beam and target polarizations, respectively. The asymmetries evaluated according to (15) were found to be consistent for the two beam helicity states. Therefore they were combined in the further analysis. Finally, the asymmetry given by (15) was unfolded for radiative and instrumental smearing effects to obtain the asymmetry corresponding to single-photon exchange in the scattering process. Radiative corrections were calculated using a Monte-Carlo generator [26]. The unfolding procedure is analogous to that used previously in other HERMES analyses [15, 27, 28]. It inflates the size

of the statistical uncertainties especially in the lowest Q^2 -bins at a given value of x . The magnitude of inflation reaches almost a factor of two at low values of x . The subdivision of x -bins in the range $x > 0.023$ into three bins in Q^2 decreases the error inflation by about a factor of 1.5 because at larger Q^2 the amount of smearing between x -bins is smaller and the prefactors of A_T in (10) and (11) are larger in magnitude. After the unfolding procedure the central values of g_2 and A_2 changed less than the initial statistical uncertainties. As a consequence of the unfolding procedure, the resulting data points are no longer correlated systematically through radiative and instrumental smearing effects, but are only statistically correlated [15]. The procedure generates a statistical covariance matrix for the data points.

In every (x, Q^2) -bin the amplitude $A_T(x, Q^2)$ was obtained by fitting the unfolded asymmetries with the function $f(\phi) = -A_T(x, Q^2) \cos \phi$. Finally, the asymmetry $A_2(x, Q^2)$ and the function $g_2(x, Q^2)$ were evaluated from the amplitude A_T and the previously measured function g_1 , for which a world-data parameterization [29] was employed, using (10) and (11). The structure function

$$F_1(x, Q^2) = F_2(x, Q^2)(1 + \gamma^2)/[2x(1 + R(x, Q^2))] \quad (18)$$

was calculated using a parameterization of the structure function $F_2(x, Q^2)$ [30] and the ratio $R(x, Q^2)$ [31]. All kinematic factors in (10) and (11), and the functions F_1 and g_1/F_1 were calculated at the average values of x and Q^2 in each (x, Q^2) -bin after unfolding.

The uncertainties in the measurements of the beam and target polarizations produce in total a 10% scale uncertainty on the value of A_T . Other sources of systematic uncertainties such as acceptance effects, small beam and spectrometer misalignments, uncertainties in the target polarization direction, correction for track deflection in the vertical target holding field, the unfolding procedure and a possible correlation between prefactors of A_T and A_T itself in (10) and (11) were evaluated by Monte-Carlo studies. Uncertainties stemming from parameterizations of $g_1(x, Q^2)$, $F_2(x, Q^2)$, and $R(x, Q^2)$ were estimated also. In the error propagation to g_2 , the uncertainty in $R(x, Q^2)$ was not included in addition to that of $F_2(x, Q^2)$, since they are strongly correlated as explained in [15]. The total systematic uncertainty was evaluated as the quadratic sum of all the considered sources. Its magnitude is less than the magnitude of the statistical uncertainty.

Figure 1 shows the values of xg_2 as a function of Q^2 for the bins with $x > 0.1$, which have sufficient coverage in Q^2 , along with results from the E143 [13] and E155 [14] experiments at SLAC. The entire set of measured data and average values of x and Q^2 are presented in Table 1. Within the accuracy of the data, they are in agreement with the other experiments. Also shown is the Wandzura–Wilczek term g_2^{WW} , which was evaluated according to (3). A world data parameterization of $g_1(x, Q^2)$ [29] was used for the calculation.

In order to study the x dependence, $A_2(x, Q^2)$ and $g_2(x, Q^2)$ in bins covering the same x range but with different Q^2 values were evolved to their mean value of Q^2

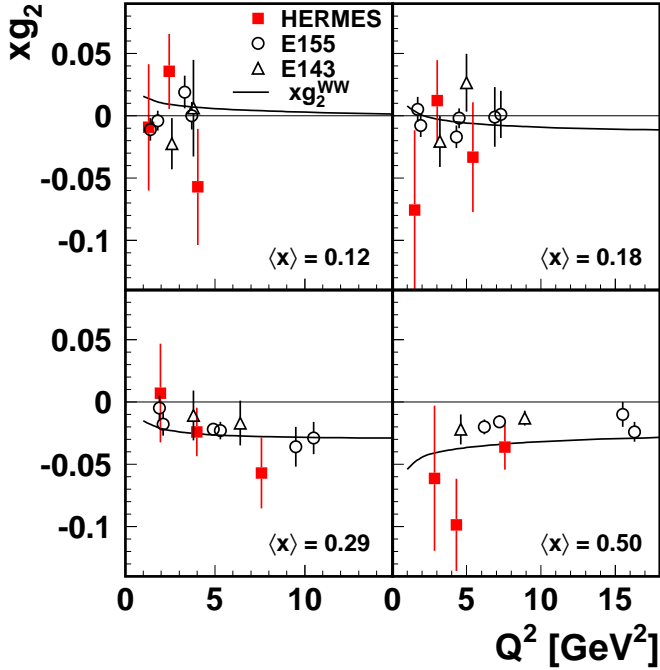


Fig. 1. The spin-structure function $xg_2(x, Q^2)$ of the proton as a function of Q^2 for selected values of x . Data from the experiments E155 [14] and E143 [13] are presented also. The average values of x for these two experiments are slightly different from the HERMES values of $\langle x \rangle$ indicated in the panels. The error bars represent the quadratic sum of the statistical and systematic uncertainties. The solid curve is the result of the Wandzura–Wilczek relation (3)

and then averaged. The evolution of $A_2(x, Q^2)$ was carried out assuming that the product $\sqrt{Q^2}A_2$ does not depend on Q^2 , which follows from (7), since g_1/F_1 is known to vary only weakly over Q^2 . The structure function $g_2(x, Q^2)$ was evolved assuming that its Q^2 dependence is analogous to that for the Wandzura–Wilczek part of g_2 .

The averaged results for xg_2 and A_2 and the statistical and systematic uncertainties are listed in Table 2, where the average values of x and Q^2 are also given. The quoted statistical uncertainties correspond to the diagonal elements of the covariance matrix obtained from the unfolding algorithm. The correlation matrix for xg_2 in nine x -bins is presented in Table 3.¹

The results for the virtual-photon asymmetry A_2 and the spin-structure function xg_2 as a function of x are presented in Fig. 2 together with data from the experiments E155 [14], E143 [13], and SMC [12]. The HERMES data are shown for two regions of Q^2 , $\langle Q^2 \rangle > 1 \text{ GeV}^2$ (closed symbols) and $\langle Q^2 \rangle < 1 \text{ GeV}^2$ (open symbols). The exper-

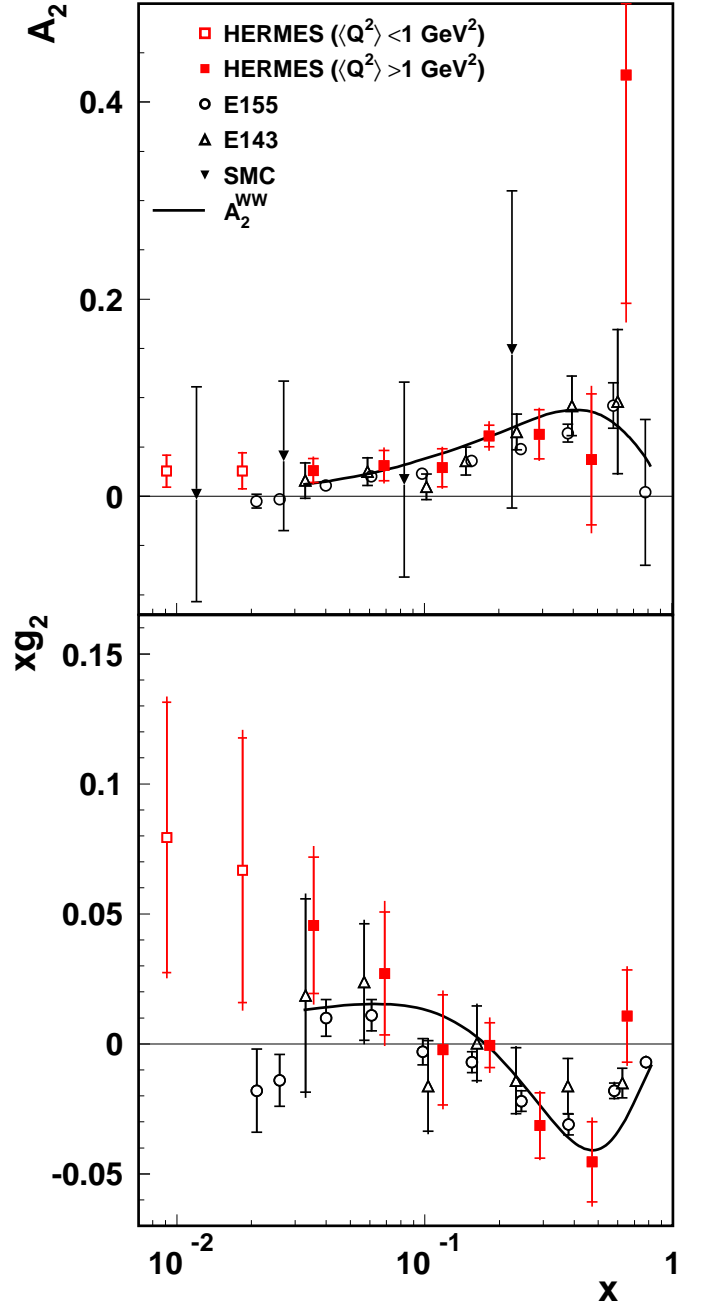


Fig. 2. Upper panel: The virtual-photon asymmetry A_2 of the proton as a function of x . Bottom panel: The spin-structure function xg_2 of the proton as a function of x . HERMES data are shown together with data from the E155 [14], E143 [13], and SMC [12] experiments. The total error bars for the HERMES, E155, and E143 experiments represent the quadratic sum of the statistical and systematic uncertainties. The statistical uncertainties are indicated by the inner error bars. The error bars for the SMC experiment represent the statistical uncertainties only. The solid curve corresponds to the Wandzura–Wilczek relation (3) evaluated at the average Q^2 values of HERMES at each value of x . For the HERMES data, the closed (open) symbols represent data with $\langle Q^2 \rangle > 1 \text{ GeV}^2$ ($\langle Q^2 \rangle < 1 \text{ GeV}^2$)

¹ It is also available in 23 bins for the data in Table 1 at <http://inspirehep.net/record/1082840> or from management@hermes.desy.de.

iments have only slightly different values of average Q^2 for a particular value of x . The results are within their uncertainties in good agreement with each other. The solid curves represent values of A_2 and xg_2 evaluated with the Wandzura–Wilczek relation (3) using the $g_1(x, Q^2)$ parameterization [29]. The values were calculated at the average Q^2 of HERMES at each value of x . Within the uncertainties the data satisfy the positivity bound [32] for the asymmetry A_2 , $|A_2| \leq \sqrt{R(1+A_1)/2} \simeq 0.4$, for all values of x in the kinematic range of the HERMES experiment.

The Burkhardt–Cottingham integral (5) was evaluated in the measured region of $0.023 \leq x < 0.9$ at $Q^2 = 5 \text{ GeV}^2$, resulting in $\int_{0.023}^{0.9} g_2(x, Q^2) dx = 0.006 \pm 0.024 \pm 0.017$. This result is to be compared with the combined result from experiments E143 and E155 [14] in the region $0.02 \leq x < 0.8$: $\int_{0.02}^{0.8} g_2(x, Q^2) dx = -0.042 \pm 0.008$.

Using the results measured by HERMES for the function g_2 , the twist-3 matrix element d_2 given by (4) was evaluated. For the unmeasured region $0.9 < x \leq 1$, the ansatz $g_2(x) \propto (1-x)^3$ was assumed. The uncertainty in the extrapolated contribution was taken to be equal to the contribution itself. The contribution from the region $x < 0.023$ was neglected because of the x^2 suppression factor. The result is $d_2 = 0.0148 \pm 0.0096(\text{stat}) \pm 0.0048(\text{syst})$. This is to be compared with the combined result from experiments E143 and E155 [14]: $d_2 = 0.0032 \pm 0.0017$.

In conclusion, HERMES measured the spin-structure function g_2 and the virtual-photon asymmetry A_2 of the proton in the kinematic range $0.004 < x < 0.9$ and $0.18 \text{ GeV}^2 < Q^2 < 20 \text{ GeV}^2$. For the covered x -range the measured integral of $g_2(x)$ converges to the null result of the Burkhardt–Cottingham sum rule. The x^2 moment of the twist-3 contribution to $g_2(x)$ is found to be compatible with zero, in agreement with expectations on its smallness from lattice calculations. The results on A_2 and g_2 are overall in good agreement with measurements of SMC at CERN, and E143 and E155 at SLAC, but they are not statistically precise enough to detect a deviation of g_2 from its Wandzura–Wilczek part, as seen by the SLAC experiments.

We gratefully acknowledge the DESY management for its support and the staff at DESY and the collaborating institutions for their significant effort. This work was supported by the Ministry of Economy and the Ministry of Education and Science of Armenia; the FWO-Flanders and IWT, Belgium; the Natural Sciences and Engineering Research Council of Canada; the National Natural Science Foundation of China; the Alexander von Humboldt Stiftung, the German Bundesministerium für Bildung und Forschung (BMBF), and the Deutsche Forschungsgemeinschaft (DFG); the Italian Istituto Nazionale di Fisica Nucleare (INFN); the MEXT, JSPS, and G-COE of Japan; the Dutch Foundation for Fundamenteel Onderzoek der Materie (FOM); the Russian Academy of Science and the Russian Federal Agency for Science and Innovations; the U.K. Engineering and Physical Sciences Research Council, the Science and Technology Facilities Council, and

the Scottish Universities Physics Alliance; the U.S. Department of Energy (DOE) and the National Science Foundation (NSF); the Basque Foundation for Science (IKERBASQUE) and the UPV/EHU under program UFI 11/55; and the European Community Research Infrastructure Integrating Activity under the FP7 "Study of strongly interacting matter (HadronPhysics2, Grant Agreement number 227431)".

References

1. M. Anselmino, A. Efremov, E. Leader, Phys. Rept. **261**, 1 (1995).
2. E.V. Shuryak and A. I. Vainshtein, Nucl. Phys. B **201**, 141 (1982).
3. R.L. Jaffe, Comments Nucl. Part. Phys. **19**, 239 (1990).
4. R.L. Jaffe and X. Ji, Phys. Rev. D **43**, 724 (1991).
5. S. Wandzura and F. Wilczek, Phys. Lett. B **72**, 195 (1977).
6. M. Gökeler *et al.*, Phys. Rev. D **63**, 074506 (2001).
7. M. Gökeler *et al.*, Phys. Rev. D **72**, 054507 (2005).
8. D.W. Sivers, Phys. Rev. D **41**, 83 (1990).
9. M. Burkardt, e-Print: arXiv:0810.3589
10. HERMES Coll., A. Airapetian *et al.*, Phys. Rev. Lett. **103**, 152002 (2009).
11. H. Burkhardt and W.N. Cottingham, Ann. Phys. **56**, 453 (1970).
12. SMC Coll., D. Adams *et al.*, Phys. Rev. D **56**, 5330 (1997).
13. E143 Coll., K. Abe *et al.*, Phys. Rev. D **58**, 112003 (1998).
14. E155 Coll., P. L. Anthony *et al.*, Phys. Lett. B **553**, 18 (2003).
15. HERMES Coll., A. Airapetian *et al.*, Phys. Rev. D **75**, 012007 (2007).
16. HERMES Coll., K. Ackerstaff *et al.*, Nucl. Instrum. Methods A **417**, 230 (1998).
17. HERMES Coll., A. Airapetian *et al.*, Nucl. Instrum. Methods A **540**, 68 (2005).
18. C. Baumgarten *et al.* (HERMES Target Group), Nucl. Instrum. Methods A **496**, 606 (2003).
19. C. Baumgarten *et al.* (HERMES Target Group), Nucl. Instrum. Methods A **508**, 633 (2003).
20. A.A. Sokolov, I.M. Ternov, Sov. Phys. Doklady **8**, 1203 (1964).
21. J. Buon and K. Steffen, Nucl. Instrum. Methods A **245**, 248 (1986).
22. D.P. Barber *et al.*, Phys. Lett. B **343**, 436 (1995).
23. D.P. Barber *et al.*, Nucl. Instrum. Methods A **329**, 79 (1993).
24. HERMES Coll., M. Beckmann *et al.*, Nucl. Instrum. Methods A **479**, 334 (2002).
25. HERMES Coll., T. Benisch *et al.*, Nucl. Instrum. Methods A **471**, 314 (2001).
26. I. Akushevich, H. Böttcher and D. Ryckbosch (1998), hep-ph/9906408.
27. HERMES Coll., A. Airapetian *et al.*, Phys. Rev. D **71**, 012003 (2005).
28. HERMES Coll., A. Airapetian *et al.*, Phys. Rev. Lett. **95**, 242001 (2005).
29. E155 Coll., P.L. Anthony *et al.*, Phys. Lett. B **493**, 19 (2000).
30. HERMES Coll., A. Airapetian *et al.*, JHEP **0511**, 126 (2011).
31. E143 Coll., K. Abe *et al.*, Phys. Lett. B **452**, 194 (1999).
32. J. Soffer and O.V. Teryaev, Phys. Lett. B **490**, 106 (2000).

Table 1. The spin-structure function $xg_2(x, Q^2)$ and the virtual-photon asymmetry $A_2(x, Q^2)$ of the proton in bins of (x, Q^2) , see text for details. Statistical and systematic uncertainties are presented separately

bin	$\langle x \rangle$	$\langle Q^2 \rangle, \text{GeV}^2$	xg_2	\pm stat.	\pm syst.	A_2	\pm stat.	\pm syst.
1	0.009	0.38	0.0799	0.0521	0.0182	0.0257	0.0163	0.0057
2	0.018	0.68	0.0699	0.0513	0.0111	0.0269	0.0183	0.0040
3	0.033	0.89	0.0450	0.0326	0.0215	0.0278	0.0165	0.0109
4	0.039	1.37	-0.0047	0.0652	0.0080	0.0033	0.0275	0.0035
5	0.044	1.80	0.3489	0.1279	0.0612	0.1440	0.0507	0.0243
6	0.067	1.09	0.0044	0.0421	0.0097	0.0190	0.0346	0.0085
7	0.069	1.88	0.0473	0.0357	0.0062	0.0402	0.0210	0.0041
8	0.076	2.79	0.0202	0.0674	0.0323	0.0225	0.0342	0.0164
9	0.116	1.30	-0.0094	0.0506	0.0081	0.0266	0.0603	0.0111
10	0.118	2.44	0.0356	0.0301	0.0099	0.0584	0.0251	0.0090
11	0.124	4.04	-0.0571	0.0466	0.0149	-0.0137	0.0311	0.0102
12	0.182	1.51	-0.0758	0.0642	0.0230	-0.0466	0.1055	0.0389
13	0.183	3.01	0.0121	0.0324	0.0038	0.0707	0.0375	0.0074
14	0.187	5.42	-0.0334	0.0440	0.0041	0.0143	0.0392	0.0052
15	0.282	1.95	0.0071	0.0396	0.0063	0.1675	0.0925	0.0167
16	0.298	3.99	-0.0242	0.0195	0.0055	0.0718	0.0363	0.0117
17	0.311	7.58	-0.0571	0.0283	0.0105	0.0039	0.0437	0.0166
18	0.458	2.83	-0.0613	0.0582	0.0129	0.0064	0.2616	0.0598
19	0.482	4.31	-0.0987	0.0370	0.0104	-0.2064	0.1704	0.0500
20	0.484	7.57	-0.0362	0.0183	0.0045	0.0421	0.0744	0.0206
21	0.630	4.76	0.2413	0.1194	0.0534	3.0231	1.3295	0.5969
22	0.658	6.79	-0.0129	0.0320	0.0081	0.1197	0.4350	0.1115
23	0.678	10.35	0.0076	0.0160	0.0025	0.3672	0.2551	0.0419

Table 2. The spin-structure function xg_2 and the virtual-photon asymmetry A_2 of the proton after evolving to common Q^2 and averaging over in each x -bin (see text for details). Statistical and systematic uncertainties are presented separately

bin	x range	$\langle x \rangle$	$\langle Q^2 \rangle, \text{GeV}^2$	xg_2	\pm stat	\pm syst	A_2	\pm stat	\pm syst
1	0.004 - 0.014	0.009	0.38	0.0794	0.0520	0.0153	0.0256	0.0162	0.0049
2	0.014 - 0.023	0.018	0.68	0.0668	0.0509	0.0181	0.0258	0.0182	0.0065
3	0.023 - 0.050	0.036	1.08	0.0456	0.0262	0.0157	0.0261	0.0121	0.0074
4	0.050 - 0.090	0.069	1.59	0.0271	0.0236	0.0150	0.0312	0.0154	0.0100
5	0.090 - 0.150	0.118	2.07	-0.0023	0.0212	0.0085	0.0289	0.0194	0.0088
6	0.150 - 0.220	0.183	2.51	-0.0005	0.0086	0.0063	0.0612	0.0109	0.0105
7	0.220 - 0.400	0.291	3.23	-0.0314	0.0126	0.0043	0.0629	0.0248	0.0104
8	0.400 - 0.600	0.473	4.62	-0.0454	0.0154	0.0075	0.0373	0.0665	0.0345
9	0.600 - 0.900	0.654	7.06	0.0107	0.0177	0.0073	0.4275	0.2316	0.0970

Table 3. Correlation matrix for xg_2 in 9 x -bins (as in Table 2)

	1	2	3	4	5	6	7	8	9
1	1.0000	-0.1281	-0.0038	-0.0033	-0.0017	0.0005	0.0000	0.0000	0.0000
2	-0.1281	1.0000	-0.1584	-0.0083	-0.0007	0.0000	0.0000	0.0001	0.0000
3	-0.0038	-0.1584	1.0000	-0.1951	-0.0281	0.0077	-0.0016	0.0002	0.0000
4	-0.0033	-0.0083	-0.1951	1.0000	-0.2885	0.0312	-0.0107	0.0013	-0.0005
5	-0.0017	-0.0007	-0.0281	-0.2885	1.0000	-0.0102	-0.0654	0.0067	-0.0018
6	0.0005	0.0000	0.0077	0.0312	-0.0102	1.0000	-0.1829	0.0143	-0.0055
7	0.0000	0.0000	-0.0016	-0.0107	-0.0654	-0.1829	1.0000	-0.3539	0.0926
8	0.0000	0.0001	0.0002	0.0013	0.0067	0.0143	-0.3539	1.0000	-0.3947
9	0.0000	0.0000	0.0000	-0.0005	-0.0018	-0.0055	0.0926	-0.3947	1.0000